Inorganic Chemistry

ARTICLE

pubs.acs.org/IC

Electronic Perturbations of Iron Dipyrrinato Complexes via Ligand *β*-Halogenation and *meso*-Fluoroarylation

Austin B. Scharf and Theodore A. Betley*

Department of Chemistry and Chemical Biology, Harvard University, 12 Oxford Street, Cambridge, Massachusetts 02138, United States

Supporting Information

ABSTRACT: Systematic electronic variations were introduced into the monoanionic dipyrrinato ligand scaffold via halogenation of the pyrrolic β-positions and/or via the use of fluorinated aryl substituents in the ligand bridgehead position in order to synthesize proligands of the type 1,9-dimesityl-β-R_4-5-Ar-dipyrrin [R = H, Cl, Br, I; Ar = mesityl, 3,5-$(F_3C)_2C_6H_3$, C_6F_5 in ligand 5-position; β = 2,3,7,8 ligand substitution; abbreviated $(^{\beta,Ar}L)H$]. The electronic perturbations were probed using standard electronic absorption and electrochemical techniques on the different ligand variations and their divalent iron complexes. The free-ligand variations cause modest shifts in the electronic absorption maxima (λ_{max}: 464−499 nm) and more pronounced shifts in the electrochemical redox potentials for one-electron proligand reductions ($E_{1/2}$: −1.25 to −1.99 V) and oxidations ($E_{1/2}$: +0.52 to +1.14 V vs $[Cp_2Fe]^{+/0}$). Installation of iron into the dipyrrinato scaffolds was effected via deprotonation of the proligands followed by treatment with $FeCl_2$ and excess pyridine in tetrahydrofuran to afford complexes of the type $(^{\beta,Ar}L)FeCl(py)$ (py = pyridine). The electrochemical and spectroscopic behavior of these complexes varies significantly across the series: the redox potential of the fully reversible $Fe^{III/II}$ couple spans more than 400 mV ($E_{1/2}$: −0.34 to +0.50 V vs $[Cp_2Fe]^{+/0}$); λ_{max} spans more than 40 nm (506−548 nm); and the ^{57}Fe Mössbauer quadrupole splitting ($|\Delta E_Q|$) spans nearly 2.0 mm/s while the isomer shift (δ) remains essentially constant (0.86−0.89 mm/s) across the series. These effects demonstrate how peripheral variation of the dipyrrinato ligand scaffold can allow systematic variation of the chemical and physical properties of iron dipyrrinato complexes.

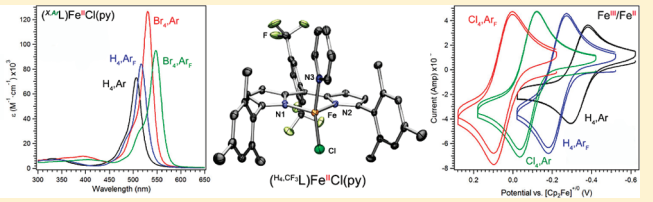

1. INTRODUCTION

The majority of research involving dipyrrins (or dipyrromethenes) has been in relation to boron difluoride dipyrrin (BODIPY) complexes, which are efficient fluorophores and have found a wide range of applications.[1] Transition metal complexes of dipyrrinato ligands have been known at least since the time of Fischer, who first developed dipyrrinato chemistry in the 1930s,[2] but have only recently received a resurgence of attention for their potential applications in metal−organic frameworks,[3] fluorescence labeling,[4] light-harvesting arrays,[5] coordination polymers,[6] and, as reported by our lab, C−H activation and functionalization chemistry.[7] While there is a vast body of literature on the effects of ligand variation on the optical properties of BODIPY dyes,[1] as well as the experimental properties of free-base and metallo-porphyrins[8] and other macrocyclic polypyrrole species,[9] there has been little systematic exploration of how peripheral ligand variations affect the chemistry of transition-metal dipyrrinato complexes.[10]

We have pursued pyrrole-based ligand platforms as truncated analogues of porphyrin and porphyrinogen ligands to examine the utility of their transition metal complexes to perform redox chemistry. The nonconjugated dipyrromethane[11] and tris(pyrrolyl)ethane platforms[12] were found to suitably bind divalent metals across the 3d series. The high-lying pyrrole-based π-electrons proved to be a liability during the examination of these complexes' redox properties. Cyclic voltammetry on the coordination complexes revealed little variation upon metal ion substitution, suggesting that the observed redox chemistry was ligand-dominated with minimal influence from the bound transition metal ion. As a result, outer-sphere electron transfer originated from the ligand pyrrole subunits, giving rise to deleterious oxidation patterns wherein the metal ion was expelled from the oxidized ligand scaffold. We therefore shifted our attention to the two-electron oxidized dipyrrin platforms, in which the conjugation of the two pyrrole subunits stabilizes the scaffold, permitting both ligand- and metal-based redox chemistry to occur without problematic decomposition.[7a] Despite both one-electron reduction and oxidation being observed for the dipyrrin scaffold itself, metal-based redox activity can also be cleanly observed. The use of the dipyrrin platform should thus permit us to investigate how systematic changes in the electronic properties of the ligand affect the bound transition metal ion. We herein report the synthesis of a series of nine dipyrrins varying at the pyrrole backbone (**2**, **3**, **7**, and **8**; or, collectively, β) positions and the bridgehead methine (5- or *meso*-) position (see Figure 1) and their Fe^{II} complexes; we also report the spectroscopic and electrochemical characterization of both the free ligands and the iron complexes.

Received: May 6, 2011
Published: June 21, 2011

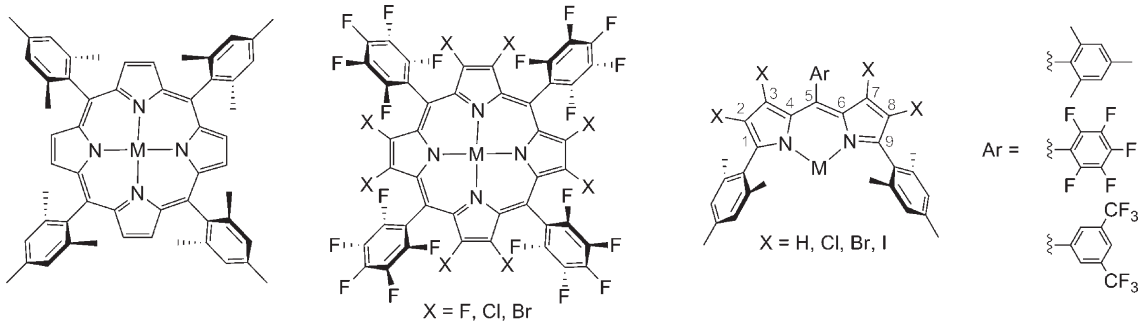

Figure 1. β-Halogenation and *meso*-fluoroarylation of porphyrins and dipyrrins.

Scheme 1. Ligand Synthesis

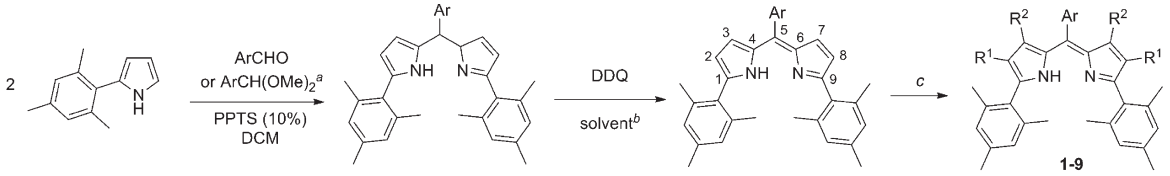

[a] For Ar = mesityl, acetal used; Ar = fluoroaryl, aldehyde used. [b] Solvent = hexanes, acetone, or CH_2Cl_2. [c] Chlorination: 6.0 equiv of *N*-chlorosuccinimide, tetrahydrofuran, 70 °C, 48 h. Bromination: *N*-bromosuccinimide, tetrahydrofuran, room temperature, 1−16 h. Iodination: excess I_2 and excess KOH, dimethylformamide, 70 °C, 48 h.

2. RESULTS AND DISCUSSION

2.1. Synthesis of Substituted Dipyrrins ($^{\beta,Ar}$L)H. Symmetrically substituted dipyrrins are synthesized via the acid-catalyzed condensation of 2 equiv of pyrrole with an aldehyde or acetal followed by oxidation with 2,3-dichloro-5,6-dicyano-1,4-benzoquinone (DDQ).[13] Our typical synthetic protocol involves reacting 2 equiv of 2-mesityl pyrrole[14] [mesityl (Mes) = 2,4,6-trimethylphenyl] with an aromatic aldehyde or acetal using pyridinium *p*-toluenesulfonate (PPTS) catalyst (10 mol %) in dichloromethane at room temperature for 12−24 h (Scheme 1). For electron-deficient aromatic aldehydes such as perfluorobenzaldehyde or 3,5-bis(trifluoromethyl)-benzaldehyde, the pyrrole condensation could be performed directly with the aldehyde in the presence of molecular sieves, whereas the reaction with mesitaldehyde dimethyl acetal was faster and higher-yielding than that with the corresponding aldehyde. The dipyrromethane products were isolated by eluting the crude reaction mixture through a silica plug to remove residual acid catalyst and highly colored byproducts and by concentrating the filtrate in vacuo. Oxidation of the dipyrromethanes was effected with DDQ (1.1 equiv, Scheme 1). Upon addition of the oxidant to the reaction solution, a color change from light yellow—characteristic of the dipyrromethanes—to dark reddish-purple was immediately observed, though the reaction was not complete for several hours. The dipyrrins (^{H_4,Mes}L)H (**1**), (^{H_4,CF_3}L)H (**6**), and (^{H_4,C_6F_5}L)H (**7**) were obtained as solids after aqueous workup. Both (^{H_4,CF_3}L)H and (^{H_4,C_6F_5}L)H required purification by chromatography on a neutral alumina column with hexanes as the eluent and were isolated as bright orange solids in 68 and 31% yields, respectively (see Table 1).

Tetrachlorination[15] of the orange-brown 5-mesityl dipyrrin (^{H_4,Mes}L)H proceeded cleanly in the presence of excess N-chlorosuccinimide (NCS, 6.6 equiv) at 70 °C in tetrahydrofuran (THF) for 24 h, over the course of which the solution turned dark red. The bright orange tetrachlorodipyrrin (^{Cl_4,Mes}L)H (**2**) was obtained after aqueous workup in 60% yield. Bromination could be achieved at room temperature with *N*-bromosuccinimide (NBS) in THF and was significantly faster than chlorination, occurring within minutes after addition of the NBS. Interestingly, dibromination of (^{H_4,Mes}L)H could be performed regioselectively at the 2- and 8-positions with strictly 2 mol equiv of NBS, affording the orange, dibrominated dipyrrin (^{Br_2,Mes}L)H (**3**) in 81% yield following workup. Crystals of **3** were grown from saturated chloroform-*d* ($CDCl_3$) solutions, permitting the determination of the dibromination regiochemistry by X-ray diffraction analysis (Figure 2). Tetrabromination of (^{H_4,Mes}L)H was also facile at room temperature in THF with excess NBS (4.4 equivalents), affording bright red (^{Br_4,Mes}L)H (**4**) in near quantitative yield under conditions identical to those employed for dibromination.[16] Iodination with

Table 1. Dipyrrin Abbreviations and Yields

	Ar	R^1/R^2	abbrev	yield of last synthetic step[a] (%)
1	Mes	H/H	(^{H_4,Mes}L)H	97
2	Mes	Cl/Cl	(^{Cl_4,Mes}L)H	60
3	Mes	Br/H	(^{Br_2,Mes}L)H	81
4	Mes	Br/Br	(^{Br_4,Mes}L)H	98
5	Mes	I/I	(^{I_4,Mes}L)H	68
6	3,5-$(CF_3)_2C_6H_3$	H/H	(^{H_4,CF_3}L)H	68
7	C_6F_5	H/H	(^{H_4,C_6F_5}L)H	31
8	C_6F_5	Cl/Cl	(^{Cl_4,C_6F_5}L)H	58
9	C_6F_5	Br/Br	(^{Br_4,C_6F_5}L)H	58

[a] For compounds **1**, **6**, and **7**, the reported yield is for DDQ oxidation; for all others, the reported yield is for halogenation.

dx.doi.org/10.1021/ic2009539 |*Inorg. Chem.* 2011, 50, 6837–6845

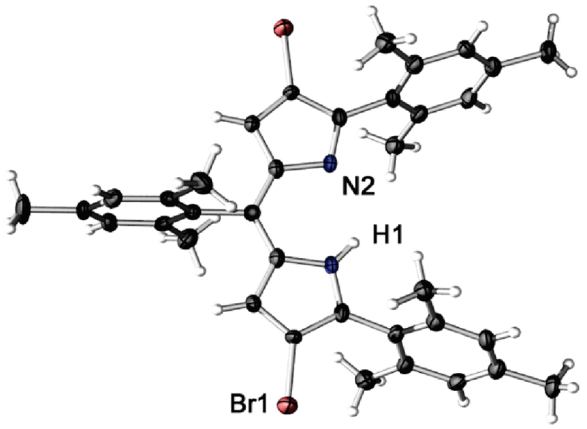

Figure 2. Regioselectivity of dibromination reaction. Solid-state molecular structure of (^{Br_2,Mes}L)H (**3**) with ellipsoids drawn at 50% probability level (C, black; H, white; N, blue; Br, brown).

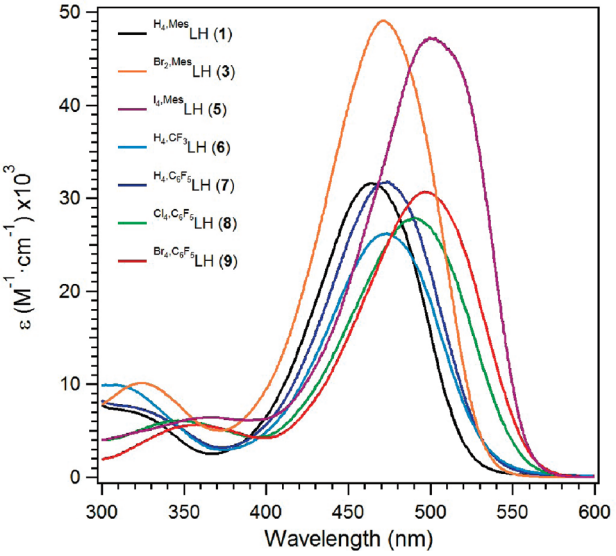

Figure 3. Representative UV/vis spectra obtained for proligands **1**, **3**, and **5**−**9**. Spectra obtained at room temperature in dichloromethane; average ε values calculated from a minimum of four concentrations.

N-iodosuccinimide gave a mixture of products, whereas reaction with I_2 under basic conditions (excess KOH) in dimethylformamide (DMF)[17] at 70 °C for 48 h gave the dark red tetraiododipyrrin (^{I_4,Mes}L)H (**5**) in good yield (67%) after workup. Unfortunately, attempts at electrophilic fluorination of the dipyrrin backbone with Selectfluor-$(BF_4)_2$[18] (which generated the boron-difluoride complex as observed by mass spectrometry), fluorination with Selectfluor-$(PF_6)_2$, or nucleophilic fluorination with AgF in dichloromethane at elevated temperatures[19] were unsuccessful.

The 5-fluoroaryl dipyrrins (^{H_4,CF_3}L)H and (^{H_4,C_6F_5}L)H were, as anticipated, less reactive toward electrophilic halogenation. Chlorination and bromination of (^{H_4,CF_3}L)H gave competitive decomposition of the compounds by an unidentified pathway (as determined by ^{1}H NMR). Halogenation of (^{H_4,C_6F_5}L)H, however, was successful, albeit with longer reaction times and lower yields than those for the 5-mesityl dipyrrin, affording red (^{Cl_4,C_6F_5}L)H (**8**) and maroon (^{Br_4,C_6F_5}L)H (**9**) in 58% yield in both cases. The 5-fluoroaryl compounds (**6**−**9**) exhibited greater solubility in nonpolar organic solvents than the 5-mesityl variants (**1**−**5**), and as such, the aqueous workup was modified (see the Supporting Information for details). After halogenation was complete (as monitored by LC-MS), the reaction solvent was removed by rotary evaporation, and the residue was dissolved in hexanes and/or ethyl acetate, washed with saturated aqueous sodium bicarbonate, water, and brine, dried over anhydrous sodium sulfate, filtered, and concentrated in vacuo to afford (^{Cl_4,C_6F_5}L)H (**8**) and (^{Br_4,C_6F_5}L)H (**9**). All ligands (**1**−**9**) were characterized by ^{1}H NMR, ^{13}C NMR, ^{19}F NMR (where applicable), UV/visible spectroscopy, and high-resolution electrospray ionization mass spectrometry (HR-ESI-MS), in which all parent molecular ions $[M + H]^+$ were detected. Full experimental details and analytical data can be found in the Supporting Information.

2.2. Characterization of Substituted Dipyrrins ($^{\beta,Ar}$L)H (1−9). Multinuclear NMR spectra (^{1}H, ^{13}C, and ^{19}F where applicable) of all the dipyrrins show C_2 symmetry on the NMR time scale, indicative of rapid tautomerization and symmetrical halogenation. The dipyrrin N−H proton is characteristically shifted downfield, ranging from 12.2 to 13.9 ppm in $CDCl_3$. Carbon−fluorine coupling constants ($^1J_{C-F}$ = 272, $^2J_{C-F}$ = 32, and $^3J_{C-F}$ = 3.8 Hz, in accord with previous reports of similar fluoroaryl groups[20]) could be obtained from the ^{13}C and ^{19}F NMR spectra of both (^{H_4,CF_3}L)H and its precursor dipyrromethane.

As π-conjugated organic molecules, dipyrrins display prominent $\pi \rightarrow \pi^*$ transitions in the visible region of the UV/visible spectrum and are consequently highly colored molecules.[21] Of the nine dipyrrins described here, the colors range from light orange [(^{H_4,Mes}L)H, (^{H_4,CF_3}L)H, and (^{H_4,C_6F_5}L)H] to maroon [(^{I_4,Mes}L)H and (^{Br_4,C_6F_5}L)H], with absorption maxima (λ_{max}) ranging from 464 nm [(^{H_4,Mes}L)H] to 499 nm [(^{I_4,Mes}L)H]. Halogenation red-shifts λ_{max} proportionally with the atomic radius of the halogen; shifts of ∼15, 20, and 35 nm are seen for tetrachlorination, bromination, and iodination, respectively (atomic radii 100, 115, and 140 pm[22]). Dibromination in **3** red-shifts λ_{max} by 7 nm, roughly half the shift seen in the case of tetrabromination in **4**. Incorporation of the fluoroaryl substituents in the 5-position has a less pronounced effect on the absorption maxima, where red-shifts of less than 10 nm are seen for both (^{H_4,CF_3}L)H and (^{H_4,C_6F_5}L)H relative to (^{H_4,Mes}L)H. The molar absorptivities (ε) of compounds **1**−**9** range from (2.5 to 4.3) × 10^4 M^{-1}·cm^{-1} with no discernible pattern related to halogenation or 5-substitution (Figure 3).

A number of reports describe the absorption spectra of chlorinated and brominated (though not, to our knowledge, iodinated) free-base porphyrins, all of which display bathochromic shifts of their absorption maxima upon halogenation, analogous to the shifts seen in our study.[8,23] Electronegative substituents such as halogens have a stabilizing effect on the energy of both the HOMO and the LUMO of conjugated systems, and when a differential stabilization of these two orbitals occurs, a shift is observed. Calculations performed by Gray and co-workers[24] and separately by Nguyen and co-workers[25] have suggested that halogenation has an approximately equivalent effect on both the HOMO and the LUMO of porphyrins, and therefore, electronic effects seem to play a minor role in the changes in the absorption spectra of these species upon halogenation. Steric effects, however, are very pronounced in halogenated porphyrins, and the introduction of chlorine or bromine

dx.doi.org/10.1021/ic2009539 |*Inorg. Chem.* 2011, 50, 6837–6845

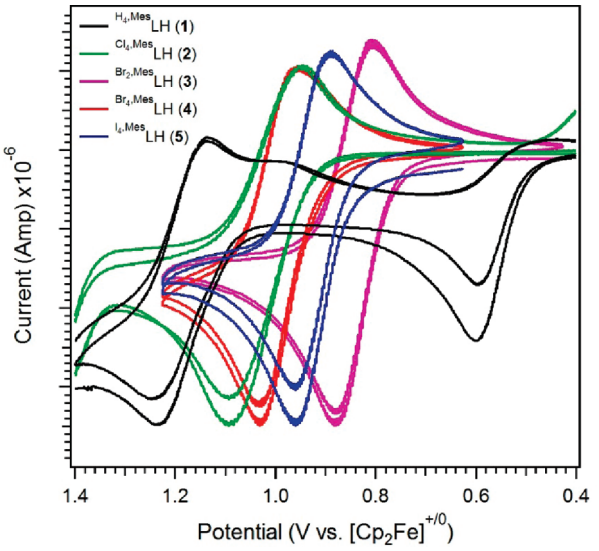

Figure 4. Effect of halogenation on dipyrrin oxidation potential. Cyclic voltammograms obtained in CH_2Cl_2 at 25 °C, with 0.1 M ($^nBu_4N$)(PF_6) as the supporting electrolyte and a scan rate of ≤250 mV/s.

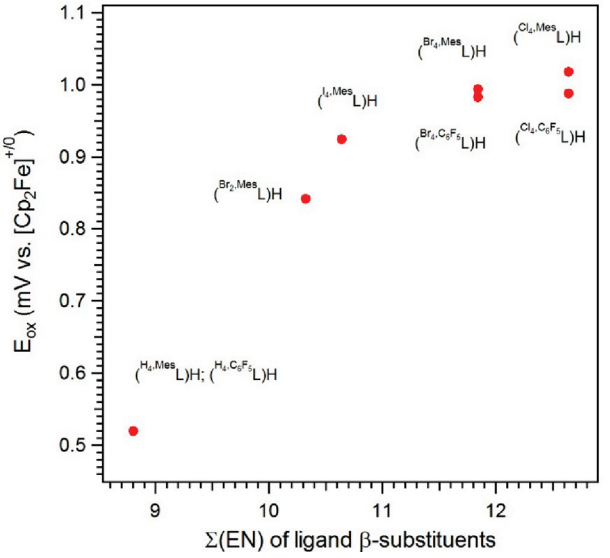

Figure 5. Correlation between electronegativity of pyrrole backbone substituents and oxidation potential. Electronegativity values taken from the ACS online periodic table[22] (H = 2.20; Cl = 3.16; Br = 2.96; I = 2.66). For reversible processes, $E_{1/2}$ is reported; for quasi- or irreversible processes, the potential at peak half-maximum is reported. Values of E_{ox} for **7**−**9** are normalized to account for the effect of 5-position variation.

substituents on the periphery leads to significant saddling distortions of the porphyrin macrocycle,[26] causing major deviations from planarity. The amplitude of these deviations correlates with the size and number of the halogen substituents, and it is to this geometric distortion that Gray and co-workers largely attribute the bathochromic shifts in the absorbance spectra.[24] It is unclear at this time whether this explanation holds for halogenated dipyrrins, which have more degrees of geometric freedom than the macrocyclic porphyrins.

Cyclic voltammetry revealed reversible or quasi-reversible oxidation events for each dipyrrin (0.1 mM analyte concentration in dichloromethane, 0.1 M ($^nBu_4N$)(PF_6), scan rate = 250 mV/s, glassy carbon working electrode, nonaqueous Ag^+/Ag reference electrode, and platinum wire counterelectrode; under a nitrogen atmosphere at ambient temperature). The onset of dipyrrin oxidation was seen at 470 mV versus [Cp_2Fe]$^{+/0}$ for the parent proligand (^{H_4,Mes}L)H, and was shifted +100 mV by the introduction of 5-fluoroaryl groups. Halogenation had a more pronounced effect on the oxidation potential of the proligand, anodically shifting the oxidation by as much as +500 mV for the most electronegative chlorine substituents (Figure 4). There was a correlation between the sum of the Pauling electronegativities of the pyrrole backbone (β position) substituents and the oxidation potential of the dipyrrin (Figure 5, Table 2); as more electronegative substituents are added to the dipyrrin backbone, the proligand becomes significantly more difficult to oxidize. The effects of 5-substitution and β-halogenation are additive; the greatest anodic shift is observed for the 5-perfluorophenyl tetrachlorodipyrrin (^{Cl_4,C_6F_5}L)H, shifting the proligand oxidation nearly +600 mV from (^{H_4,Mes}L)H. In the cases of the nonhalogenated compounds [(^{H_4,Mes}L)H, (^{H_4,CF_3}L)H, and (^{H_4,C_6F_5}L)H], a second one-electron, quasi-reversible oxidation event could be observed (see Figures S19, S24, and S25 in the Supporting Information).

Electrochemical reduction of the ligands was also reversible or quasi-reversible across the series, with the exception of (^{Cl_4,C_6F_5}L)H, for which reduction was irreversible. The parent proligand (^{H_4,Mes}L)H was the most difficult to reduce, with $E_{1/2}$ = −2.0 V vs [Cp_2Fe]$^{+/0}$. Introduction of electron-withdrawing substituents in the β- and/or 5-position made reduction more facile. 5-Fluoroarylation shifted the reduction potentials by +100 to +200 mV, and tetrahalogenation shifted the reduction potential by roughly +450 mV. It is interesting to note that most of these reduction events are reversible, indicating that stable halide anions are not expelled on the time-scale of the voltammetric experiment. Cyclic voltammograms can be found in the Supporting Information (Figures S19−S27). The redox activity of the nonmetalated proligands indicates the potential for ligand participation in redox processes of the derivative iron complexes. Explorations of this reactivity are currently underway in our lab.

Studies of the redox properties of dipyrrins are numerous in the early literature, where both oxidation and reduction events have been recorded for the vast majority of species,[21,27] but there have been, to our knowledge, no reports on the effect of halogenation on these redox properties. There are, however, several studies of the redox properties of halogenated porphyrins,[24,28] and the trends in such systems parallel those observed for halogenated dipyrrins, where the β-incorporation of halogens anodically shifts both ligand oxidation and reduction processes where a correlation can be drawn to the electronegativity of the halogen. Similar studies have shown the effects of *meso*-fluoroarylation of porphyrins,[29] again paralleling the trends observed for the dipyrrins in this study.

2.3. Synthesis of Fe Complexes ($^{\beta,Ar}$L)FeCl(py). Initially, tetrahydrofuran adducts of iron dipyrrinato complexes were targeted,[7a] but these species did not exhibit the stability desired to acquire a full suite of spectroscopic data, as significant decomposition of the complexes (even in the solid state) was apparent after several days. As such, the less labile pyridine adducts were targeted to record all the metrical data presented herein. Under a nitrogen atmosphere, deprotonation of the proligands (**1**−**9**) (see Scheme 2) with 1 equiv of lithium hexamethyldisilazide in thawing THF at 77 K afforded the lithium salts, which have been

dx.doi.org/10.1021/ic2009539 |*Inorg. Chem.* 2011, 50, 6837–6845

Table 2. Characterization Data of Dipyrrin Proligands

	Ar	R^1/R^2	abbrev	λ_{max}[a] (nm)	ε[b] ($M^{-1}\cdot cm^{-1}$)	$E_{1/2}$(ox)[c] (V)	$E_{1/2}$(red)[c] (V)	ΣEN[e] (Pauling)
1	Mes	H/H	$(^{H_4,Mes}L)H$	464.0	31,000	0.520[d]	−1.999	8.80
2	Mes	Cl/Cl	$(^{Cl_4,Mes}L)H$	480.0	36,000	1.018	−1.558	12.64
3	Mes	Br/H	$(^{Br_2,Mes}L)H$	471.0	38,000	0.842	−1.763	10.32
4	Mes	Br/Br	$(^{Br_4,Mes}L)H$	485.0	26,000	0.994	−1.544	11.84
5	Mes	I/I	$(^{I_4,Mes}L)H$	499.4	43,000	0.925	−1.547	10.64
6	3,5-$(CF_3)_2C_6H_3$	H/H	$(^{H_4,CF_3}L)H$	472.0	27,000	0.636[d]	−1.720	8.80
7	C_6F_5	H/H	$(^{H_4,C_6F_5}L)H$	473.0	32,000	0.676[d]	−1.707	8.80
8	C_6F_5	Cl/Cl	$(^{Cl_4,C_6F_5}L)H$	490.0	27,000	1.144	−1.264[d]	12.64
9	C_6F_5	Br/Br	$(^{Br_4,C_6F_5}L)H$	497.0	31,000	1.139	−1.251	11.84

[a] UV/vis spectra obtained in dichloromethane at 25 °C with a maximum scan rate of 600 nm/min. [b] Average extinction coefficients calculated from a minimum of four concentrations. [c] Cyclic voltammetry performed in dichloromethane containing 0.1 M ($^nBu_4N$)(PF_6) at 25 °C and a maximum scan rate of 250 mV/s; referenced vs $[Cp_2Fe]^{+/0}$. [d] Irreversible; values reported are the potentials at peak half-maximum. [e] The sum of the Pauling electronegativity values of the β position substituents, taken from the ACS online periodic table; H = 2.20, Cl = 3.16, Br = 2.96, I = 2.66.[22]

Scheme 2. Deprotonation and Metalation

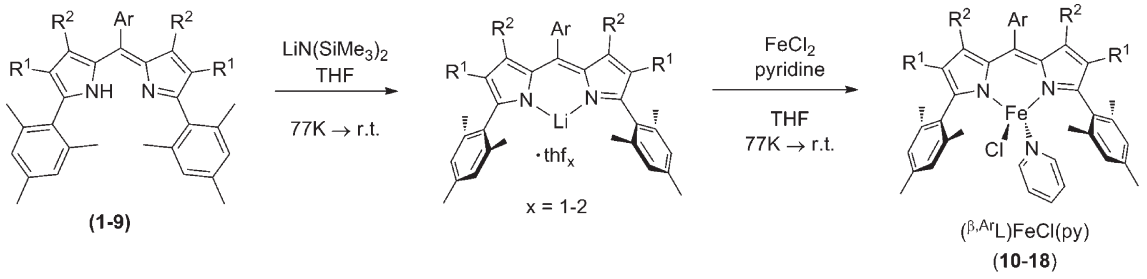

shown to be effective precursors for transmetalation to transition metals[7,30] (^{1}H NMR spectral data are presented in the Supporting Information). After concentration in vacuo, the salts were isolated as dark red THF adducts with 1−2 molecules of THF coordinating the Li, as determined by ^{1}H NMR spectroscopy. Reaction of the lithium salts with 1.1 equiv of $FeCl_2$ in thawing THF solutions in the presence of excess pyridine effected transmetalation to iron. The mixtures were concentrated to dryness in vacuo, dissolved in benzene, filtered through a plug of diatomaceous earth to remove insoluble material, and again concentrated to dryness. Washing the complexes with a minimal amount of cold (−35 °C) hexanes or hexamethyldisiloxane afforded the clean iron complexes in the following good yields (51−95%): $(^{H_4,Mes}L)FeCl(py)$ (**10**, 95%); $(^{Cl_4,Mes}L)FeCl(py)$ (**11**, 77%); $(^{Br_2,Mes}L)FeCl(py)$ (**12**, 81%); $(^{Br_4,Mes}L)FeCl(py)$ (**13**, 67%); $(^{I_4,Mes}L)FeCl(py)$ (**14**, 51%); $(^{H_4,CF_3}L)FeCl(py)$ (**15**, 89%, the structure of which is shown in Figure 6); $(^{H_4,C_6F_5}L)FeCl(py)$ (**16**, 87%); $(^{Cl_4,C_6F_5}L)FeCl(py)$ (**17**, 81%); $(^{Br_4,C_6F_5}L)FeCl(py)$ (**18**, 76%). In some cases, trace amounts (<5%) of free ligand remained. The iron complexes ranged from dark orange—$(^{H_4,Mes}L)FeCl(py)$, $(^{H_4,CF_3}L)FeCl(py)$, and $(^{H_4,C_6F_5}L)FeCl(py)$—to very dark pink—$(^{I_4,Mes}L)FeCl(py)$ and $(^{Br_4,C_6F_5}L)FeCl(py)$—in solution and as amorphous solids, but the were lustrous green to green-brown solids in the microcrystalline state. All complexes were characterized by ^{1}H NMR, ^{19}F NMR (where applicable), UV/visible spectroscopy, cyclic voltammetry, ^{57}Fe Mössbauer spectroscopy, and combustion analysis (see the Supporting Information for details).

2.4. Multinuclear NMR Spectra of $(^{\beta,Ar}L)FeCl(py)$ Complexes. ^{1}H NMR spectra of all complexes in the series showed

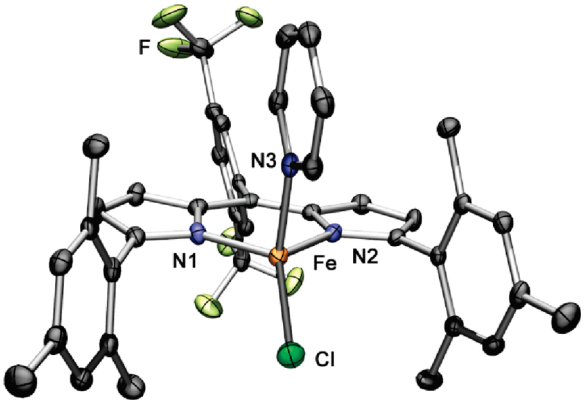

Figure 6. Solid-state molecular structure of $(^{H_4,CF_3}L)FeCl(py)$ (**15**) with ellipsoids drawn at the 50% probability level (H atoms omitted for clarity; C, black; N, blue; Fe, orange; F, yellow-green; Cl, green). Bond lengths (Å) for **15**: Fe−N1, 2.026(2); Fe−N2, 2.030(2); Fe−N3, 2.098(2); Fe−Cl, 2.2304(8).

significant paramagnetic broadening due to the presence of high-spin Fe^{II} ($S = 2$);[31] typical spectra were observed in a spectral window of −40 to +60 ppm. Complexes with 5-fluoroaryl substituents (**15**−**18**) gave useful ^{19}F NMR spectra as well. In the case of $(^{H_4,CF_3}L)FeCl(py)$ (**15**), the two trifluoromethyl groups gave rise to two distinct signals, indicating an unexpected lack of free rotation of the bis(trifluoromethyl)phenyl substituent. The corresponding ^{1}H NMR spectrum also displayed more paramagnetically shifted peaks than anticipated, but with the

dx.doi.org/10.1021/ic2009539 |Inorg. Chem. 2011, 50, 6837–6845

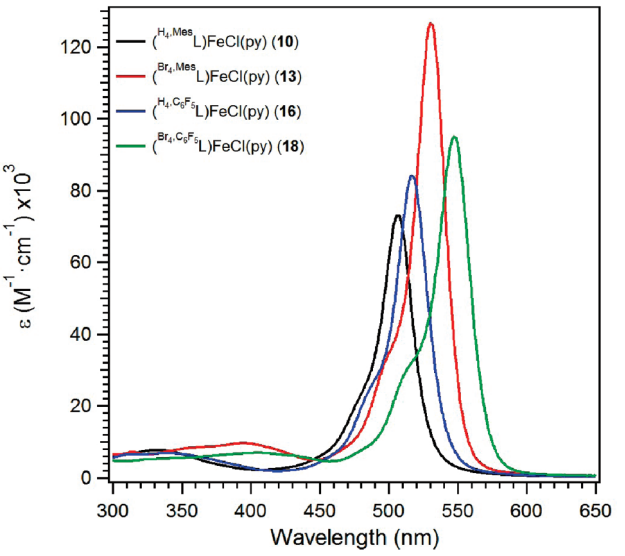

Figure 7. Representative UV/vis spectra for complexes **10**, **13**, **16**, and **18**. Spectra obtained at room temperature in dichloromethane; average ε values calculated from a minimum of four concentrations.

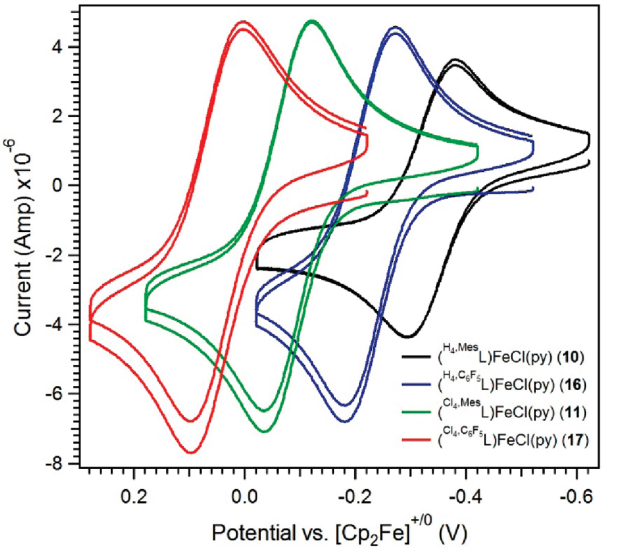

Figure 8. $Fe^{III/II}$ couples of representative complexes. Cyclic voltammograms obtained in THF with 0.3 M ($^nBu_4N$)(PF_6) as supporting electrolyte with a scan rate of 100 mV/s.

larger number of peaks and spectral broadening, the inequivalent *ortho*-hydrogen peaks could not be unambiguously identified. The 5-perfluorophenyl dipyrrinato complexes **16**−**18** ($^{\beta,C_6F_5}$L)FeCl(py) uniformly showed three peaks for the aryl fluorine nuclei, indicating that rotation in these complexes is not hindered as in **15**, although there is precedent for lack of free rotation observed in octahalogenated *meso*-tetrakis(perfluorophenyl) porphyrins.[32] The peak for the *para*-fluorine was consistently sharp, but the *meta*- and *ortho*-fluorine peaks were affected by paramagnetic broadening due to their closer proximity to the Fe^{II} center.[33]

2.5. Electronic Absorption Spectra of ($^{\beta,Ar}$L)FeCl(py) Complexes. Each of the iron complexes displayed two prominent absorption bands in the UV/visible region, both attributable to

Table 3. Yields of Iron Complexes

	abbrev	Ar	R^1/R^2	yield (%)
10	(^{H_4,Mes}L)FeCl(py)	Mes	H/H	95
11	(^{Cl_4,Mes}L)FeCl(py)	Mes	Cl/Cl	77
12	(^{Br_2,Mes}L)FeCl(py)	Mes	Br/H	81
13	(^{Br_4,Mes}L)FeCl(py)	Mes	Br/Br	67
14	(^{I_4,Mes}L)FeCl(py)	Mes	I/I	51
15	(^{H_4,CF_3}L)FeCl(py)	3,5-$(CF_3)_2C_6H_3$	H/H	89
16	(^{H_4,C_6F_5}L)FeCl(py)	C_6F_5	H/H	87
17	(^{Cl_4,C_6F_5}L)FeCl(py)	C_6F_5	Cl/Cl	81
18	(^{Br_4,C_6F_5}L)FeCl(py)	C_6F_5	Br/Br	76

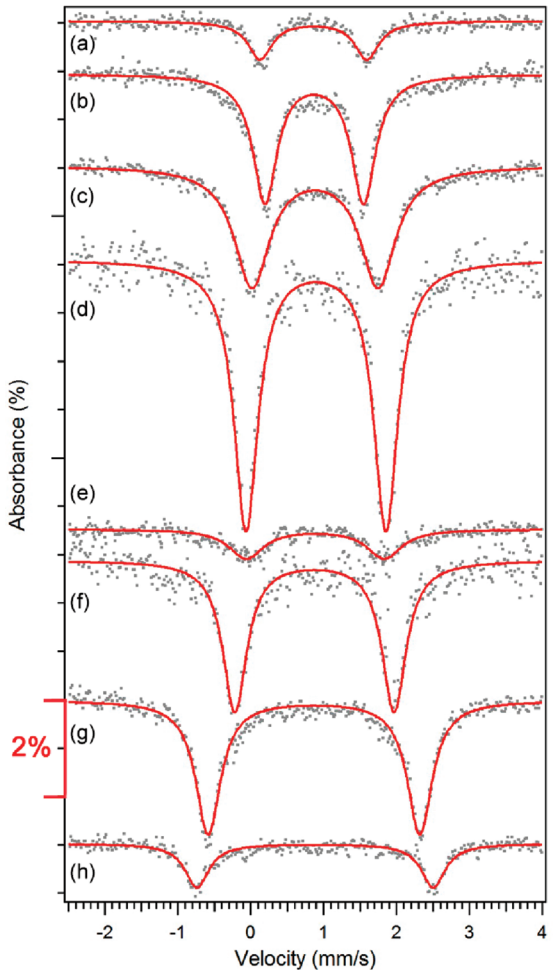

Figure 9. Zero-field ^{57}Fe Mössbauer spectra obtained at 110 K for the following compounds: (^{Br_2,Mes}L)FeCl(py), **12** (a); (^{Cl_4,C_6F_5}L)FeCl(py), **17** (b); (^{H_4,CF_3}L)FeCl(py), **15** (c); (^{H_4,C_6F_5}L)FeCl(py), **16** (d); (^{I_4,Mes}L)FeCl(py), **14** (e); (^{H_4,Mes}L)FeCl(py), **10** (f); (^{Cl_4,Mes}L)FeCl(py), **11** (g); and (^{Br_4,Mes}L)FeCl(py), **13** (h).

primarily ligand-based $\pi \rightarrow \pi^*$ transitions.[34] The less intense of the two absorptions is red-shifted from the free ligand absorption bands and appears as a shoulder under the more prominent, slightly lower-energy $\pi \rightarrow \pi^*$ transition. The more intense $\pi \rightarrow \pi^*$ absorptions ($\varepsilon = 5.4 \times 10^4$ to 1.3×10^5 M^{-1} cm^{-1}) occur with the absorption maxima ranging from 506 nm for (^{H_4,Mes}L)FeCl(py) (**10**) to 548 nm for (^{Br_4,C_6F_5}L)FeCl(py) (**18**)

dx.doi.org/10.1021/ic2009539 |*Inorg. Chem.* 2011, 50, 6837–6845

Table 4. Characterization Data of Iron Dipyrrinato Complexes (10−18)

	abbrev	Ar	R^1/R^2	$E_{1/2}$ $Fe^{III/II}$ [a] (mV)	λ_{max} [b] (nm)	ε [c] ($M^{-1}\cdot cm^{-1}$)	δ [d] (mm/s)	$\lvert\Delta E_Q\rvert$ (mm/s)
10	$(^{H_4,Mes}L)FeCl(py)$	Mes	H/H	−336	506.0	73,000	0.87	2.19
11	$(^{Cl_4,Mes}L)FeCl(py)$	Mes	Cl/Cl	−79	524.5	83,000	0.87	2.9
12	$(^{Br_2,Mes}L)FeCl(py)$	Mes	Br/H	−154	528.0	97,000	0.86[e]	1.46[e]
13	$(^{Br_4,Mes}L)FeCl(py)$	Mes	Br/Br	−95	530.5	130,000	0.88[e]	3.24[e]
14	$(^{I_4,Mes}L)FeCl(py)$	Mes	I/I	−170	545.6	83,000	0.89[e]	1.89[e]
15	$(^{H_4,CF_3}L)FeCl(py)$	3,5-$(CF_3)_2C_6H_3$	H/H	−238	508.5	62,000	0.89	1.74
16	$(^{H_4,C_6F_5}L)FeCl(py)$	C_6F_5	H/H	−227	516.7	84,000	0.89	1.92
17	$(^{Cl_4,C_6F_5}L)FeCl(py)$	C_6F_5	Cl/Cl	+50	541.5	54,000	0.87	1.35
18	$(^{Br_4,C_6F_5}L)FeCl(py)$	C_6F_5	Br/Br	+20	547.5	95,000	[f]	[f]

[a] Cyclic voltammetry performed in THF containing 0.3 M $(^nBu_4N)(PF_6)$ at 25 °C. [b] UV/vis spectra obtained in CH_2Cl_2 at 25 °C with a scan rate of 300 nm/min. [c] Average extinction coefficients calculated from a minimum of four concentrations. [d] Mössbauer spectra obtained on samples suspended in Paratone at 110 K and fit with Lorentzian functions in IGOR Pro. [e] Bromine- and iodine-containing samples showed poor Mössbauer absorbance at 110 K and a variety of concentrations, so signal-to-noise ratios were poor for these samples; however, the fits obtained were reproducible. [f] The signal-to-noise ratio of **18** was too poor to obtain reproducible Mössbauer parameters.

(Figure 7) and follow patterns analogous to those described for the proligands (vide supra).

The optical properties of dipyrrinato-metal complexes are of particular importance, as these complexes are receiving attention as fluorophores[4a,c,35] and phosphorophores.[36] While our iron complexes do not display any appreciable fluorescence or phosphorescence, the ability to tune absorption maxima by simple transformations such as β-halogenation or 5-fluoroaryl substitution may have implications for the analogous systems. Additionally, incorporation of bromine or iodine provides a functional group handle for the synthesis of other dipyrrinato derivatives (by metal-catalyzed cross-coupling reactions), which may allow for a wider range of wavelengths, absorptivities, and emissivities to be accessed.

2.6. Cyclic Voltammetry of $(^{\beta,Ar}L)FeCl(py)$ Complexes. The iron complexes in this study (**10**−**18**) showed fully reversible $Fe^{III/II}$ couples by cyclic voltammetry (0.1 mM analyte concentration in THF, 0.3 M $(^nBu_4N)(PF_6)$, scan rate = 100 mV/s, glassy carbon working electrode, nonaqueous Ag^+/Ag reference electrode, and platinum wire counterelectrode; under a nitrogen atmosphere at ambient temperature; Figures S28−S36 in the Supporting Information). Both β-halogenation and 5-fluoroaryl substitution anodically shift the oxidation potential of the complexes relative to that of the parent complex $(^{H_4,Mes}L)FeCl(py)$. Representative complexes from the series **10**−**18** are shown overlaid in Figure 8. The introduction of a 5-fluoroaryl group raised the oxidation potential by roughly +100 mV, while β-halogenation raised the potential by +257 mV in $(^{Cl_4,Mes}L)FeCl(py)$ (**11**), +182 mV in $(^{Br_4,Mes}L)FeCl(py)$ (**12**), +241 mV in $(^{Br_4,Mes}L)FeCl(py)$ (**13**), and +166 mV in $(^{I_4,Mes}L)FeCl(py)$ (**14**), where less electronegative halogens impart a smaller anodic shift. As in the nonmetalated dipyrrin proligands, these effects were additive, and the most difficult species to oxidize was $(^{Cl_4,C_6F_5}L)FeCl(py)$ (**17**), which displays a +386 mV anodic shift from the parent compound $(^{H_4,Mes}L)FeCl(py)$ (**10**).

2.7. Zero-Field ^{57}Fe Mössbauer Spectroscopy of $(^{\beta,Ar}L)FeCl(py)$ Complexes. Acquisition of zero-field ^{57}Fe Mössbauer spectra was slow because of the poor absorbance of several samples due to the relatively low percent by mass of iron in the brominated and iodinated complexes, as well as the low Debye temperature of tetrahedral Fe^{II} complexes.[37] However, acceptable spectra could be obtained with 80−100 mg of these complexes at 110 K[38] and acquisition times of several days. Spectra of the β-protio and β-chlorinated samples could be obtained much more rapidly and with smaller samples (40−50 mg). The spectrum for the parent complex $(^{H_4,Mes}L)FeCl(py)$ (**10**) contains a single quadrupole doublet that can be modeled with parameters typical of high-spin, tetrahedral Fe^{II} complexes: δ = 0.87 mm/s and $\lvert\Delta E_Q\rvert$ = 2.19 mm/s. The isomer shifts (δ) of the other complexes in this series were nearly constant and varied by no more than 0.02 mm/s from those for **10** (see Table 3 for spectral parameters), which is consistent with an Fe^{II} formulation despite the potential for ligand-based redox activity as demonstrated by cyclic voltammetry (vide supra). Though there was little perturbation of the isomer shift for complexes **10**−**18**, the quadrupole splitting parameters ($\lvert\Delta E_Q\rvert$) for the series span a range of values, from a minimum of 1.35 mm/s for $(^{Cl_4,C_6F_5}L)FeCl(py)$ to a maximum of 3.24 mm/s for $(^{Br_4,Mes}L)FeCl(py)$ (see Figure 9 and Table 4). Although both the absorption maxima and cyclic voltammetry data varied as a function of β-halogen size and/or electronegativity, no correlation for the quadrupole splitting based on these considerations was immediately forthcoming. Quadrupole splitting reflects the electric field gradient at the iron nucleus and is therefore a function of the asymmetry around the iron center and the geometry of the complex.[39] We surmise that the β-halogenation gives rise to significant geometric variation within the series, accounting for the large range of quadrupole splitting parameters observed.

3. CONCLUSIONS

Systematic electronic variations were introduced into the monoanionic dipyrrin ligand scaffold via halogenation of the pyrrolic β-positions and/or via the use of fluorinated aryl substituents in the ligand bridgehead position yielding proligands of the type $(^{\beta,Ar}L)H$. The electronic perturbations were probed using standard spectroscopic and electrochemical techniques on the different proligand variations and their divalent iron complexes. The proligand variations display modest shifts in the electronic absorption maxima and a more pronounced effect in the electrochemical redox potentials for the one-electron ligand reductions and oxidations. The electrochemical and spectroscopic behavior of the iron-bound complexes varies significantly across the series; most notably the redox potential of the fully reversible $Fe^{III/II}$ couple spans more than 400 mV as electron-withdrawing substituents are appended to the dipyrrinato platform.

dx.doi.org/10.1021/ic2009539 |Inorg. Chem. 2011, 50, 6837–6845

These effects demonstrate how the peripheral variation of the dipyrrinato ligand scaffold can allow the systematic variation of the chemical and physical properties of iron dipyrrinato complexes. This last observation is in stark contrast to the nonconjugated dipyrromethane and tris(pyrrolyl)ethane metal complexes which show no variation in the ligand-based redox behavior regardless of the complex metal-ion inclusion, complex spin-state, or geometry.

■ ASSOCIATED CONTENT

Supporting Information. General experimental considerations; experimental details; ^{1}H, ^{13}C, and ^{19}F NMR spectra; UV/visible spectra; cyclic voltammograms; Mössbauer spectra; and X-ray crystallographic data for **3**. This material is available free of charge via the Internet at http://pubs.acs.org.

■ AUTHOR INFORMATION

Corresponding Author
*E-mail: betley@chemistry.harvard.edu.

■ ACKNOWLEDGMENT

The authors thank the NSF (CHE-0955885) and Harvard University for financial support; Guy Edouard, Danielle Raad, Sam Goldstein, and Evan King for the synthesis of starting materials; Graham Sazama, Dr. Alison Fout, and Dr. Shao-Liang Zheng for assistance with X-ray diffraction studies; Dr. Richard Holm for the use of the Mössbauer spectrometer; and Dr. Yu-Sheng Chen at ChemMatCARS, APS, for his assistance with single-crystal data. ChemMatCARS Sector 15 is principally supported by the National Science Foundation/Department of Energy under Grant No. NSF/CHE-0822838. Use of the Advanced Photon Source was supported by the U.S. Department of Energy, Office of Science, Office of Basic Energy Sciences, under Contract No. DE-AC02-06CH11357.

■ REFERENCES

(1) (a) Benniston, A. C.; Copley, G. *Phys. Chem. Chem. Phys.* **2009**, *11*, 4124–4131. (b) Loudet, A.; Burgess, K. *Chem. Rev.* **2007**, *107*, 4891–4932. (c) Ulrich, G.; Ziessel, R.; Harriman, A. *Angew. Chem., Int. Ed.* **2008**, *47*, 1184–1201. (d) Ziessel, R.; Ulrich, G.; Harriman, A. *New J. Chem.* **2007**, *31*, 496–501.

(2) Fischer, H.; Orth, H. *Die Chemie des Pyrrols*; Akademische Verlagsgesellschaft MBH: Leipzig, 1937; Vol. 2.

(3) (a) Cohen, S. M.; Halper, S. R. *Inorg. Chim. Acta* **2002**, *341*, 12–16. (b) Murphy, D. L.; Malachowski, M. R.; Campana, C. F.; Cohen, S. M. *Chem. Commun.* **2005**, *44*, 5506–5508. (c) Stork, J. R.; Thoi, V. S.; Cohen, S. M. *Inorg. Chem.* **2007**, *46*, 11213–11223. (d) Halper, S. R.; Cohen, S. M. *Inorg. Chem.* **2005**, *44*, 486–488.

(4) (a) Filatov, M. A.; Lebedev, A. Y.; Mukhin, S. N.; Vinogradov, S. A.; Cheprakov, A. V. *J. Am. Chem. Soc.* **2010**, *132* (28), 9552–9554. (b) Ikeda, C.; Ueda, S.; Nabeshima, T. *Chem. Commun.* **2009**, 2544–2546. (c) Wilson, C. J.; James, L.; Mehl, G. H.; Boyle, R. W. *Chem. Commun.* **2008**, 4582–4584.

(5) Yu, L.; Muthukumaran, K.; Sazanovich, I. V.; Kirmaier, C.; Hindin, E.; Diers, J. R.; Boyle, P. D.; Bocian, D. F.; Holten, D.; Lindsey, J. S. *Inorg. Chem.* **2003**, *42* (21), 6629–6647.

(6) (a) Halper, S. R.; Malachowski, M. R.; Delaney, H. M.; Cohen, S. M. *Inorg. Chem.* **2004**, *43* (4), 1242–1249. (b) Do, L.; Halper, S. R.; Cohen, S. M. *Chem. Commun.* **2004**, 2662–2663.

(7) (a) King, E. R.; Betley, T. A. *Inorg. Chem.* **2009**, *48*, 2361–2363. (b) King, E. R.; Hennessy, E. T.; Betley, T. A. *J. Am. Chem. Soc.* **2011**, *133*, 4917–4923.

(8) Kadish, K. M.; Smith, K. M.; Guilard, R. *The Porphyrin Handbook*; Academic Press: New York, 2003; Vol. 1−20.

(9) (a) Vogel, E. *Pure Appl. Chem.* **1996**, *68*, 1355–1360. (b) Vogel, E. *Pure Appl. Chem.* **1990**, *62*, 557–564. (c) Srinivasan, A.; Furuta, H. *Acc. Chem. Res.* **2005**, *38*, 10–20. (d) Paolesse, R. *Synlett* **2008**, *15*, 2215–2230. (e) Rio, Y.; Rodríguez-Morgade, M. S.; Torres, T. *Org. Biomol. Chem.* **2008**, *6*, 1877–1894. (f) Lash, T. D. *Eur. J. Org. Chem.* **2007**, 5461–5481. (g) Chmielewski, P. J.; Latos-Grażyński, L. *Coord. Chem. Rev.* **2005**, *249*, 2510–2533.

(10) Wood, T. E.; Thompson, A. *Chem. Rev.* **2007**, *107*, 1831–1861.

(11) King, E. R.; Betley, T. A. *J. Am. Chem. Soc.* **2009**, *131*, 14373–14380.

(12) Sazama, G. T.; Betley, T. A. *Inorg. Chem.* **2010**, *49*, 2512–2524.

(13) Fischer, H.; Elhardt, E. *Z. Physiol. Chem.* **1939**, *257*, 61–105.

(14) Rieth, R. D.; Mankad, N. P.; Calimano, E.; Sadighi, J. P. *Org. Lett.* **2004**, *6*, 3981–3983.

(15) Bhyrappa, P.; Sankar, M.; Varghese, B. *Inorg. Chem.* **2006**, *45*, 4136–4149.

(16) Chumakov, D. E.; Khoroshutin, A. V.; Anisimov, A. V.; Kobrakov, K. I. *Chem. Heterocycl. Compd.* **2009**, *45*, 259–283.

(17) Gupton, J. T.; Banner, E. J.; Scharf, A. B.; Norwood, B. K.; Kanters, R. P. F.; Dominey, R. N.; Hempel, J. E.; Kharlamova, A.; Bluhn-Chertudi, I.; Hickenboth, C. R.; Little, B. A.; Sartin, M. D.; Coppock, M. B.; Krumpe, K. E.; Burnham, B. S.; Holt, H.; Du, K. X.; Keertikar, K. M.; Diebes, A.; Ghassemi, S.; Sikorski, J. A. *Tetrahedron* **2006**, *62*, 8243–8255.

(18) Suydam, I. T.; Strobel, S. A. *J. Am. Chem. Soc.* **2008**, *130*, 13639–13648.

(19) Tsuchiya, S.; Seno, M. *Chem. Lett.* **1989**, 263–266.

(20) Yakelis, N. A.; Bergman, R. G. *Organometallics* **2005**, *24*, 3579–3581.

(21) Falk, H. *The Chemistry of Linear Oligopyrroles and Bile Pigments*; Springer-Verlag Wien: New York, 1989.

(22) ACS Online Periodic Table. http://acswebcontent.acs.org/games/pt.html.

(23) Chumakov, D. E.; Khoroshutin, A. V.; Anisimov, A. V.; Kobrakov, K. I. *Chem. Heterocycl. Compd.* **2009**, *45*, 259–283.

(24) Takeuchi, T.; Gray, H. B; Goddard, W.A., III. *J. Am. Chem. Soc.* **1994**, *116*, 9730–9732.

(25) Nguyen, K. A.; Day, P. N.; Pachter, R. *J. Chem. Phys.* **1999**, *110* (18), 9135–9144.

(26) Mandon, D.; Ochsenbein, P.; Fischer, J.; Weiss, R.; Jayaraj, K.; Austin, R. N.; Gold, A.; White, P. S.; Brigaud, O.; Battioni, P.; Mansuy, D. *Inorg. Chem.* **1992**, *31*, 2044–2049.

(27) Ribo, J. M.; Farrera, J.-A.; Claret, J.; Grubmayr, K. *Bioelectrochem. Bioenerg.* **1992**, *29*, 1–17.

(28) (a) Grinstaff, M. W.; Hill, M. G.; Birnbaum, E. R.; Schaefer, W. P.; Labinger, J. A.; Gray, H. B. *Inorg. Chem.* **1995**, *34*, 4896–4902. (b) Kadish, K. M.; Lin, M.; Caemelbecke, E. V.; Stefano, G. D.; Medforth, C. J.; Nurco, D. J.; Nelson, N. Y.; Krattinger, B.; Muzzi, C. M.; Jaquinod, L.; Xu, Y.; Shyr, D. C.; Smith, K. M.; Shelnutt, J. A. *Inorg. Chem.* **2002**, *41*, 6673–6687.

(29) Hodge, J. A.; Hill, M. G.; Gray, H. B. *Inorg. Chem.* **1995**, *34*, 809–812.

(30) (a) Cipot-Wechsler, J.; Ali, A. A.-S.; Chapman, E. E.; Cameron, T. S.; Thompson, A. *Inorg. Chem.* **2007**, *46*, 10947–10949. (b) Ali, A. A-S.; Cipot-Wechsler, J.; Crawford, S. M.; Selim, O.; Stoddard, R. L.; Cameron, T. S.; Thompson, A. *Can. J. Chem.* **2010**, *88*, 725–735.

(31) La Mar, G. N.; Horrocks, W. D., Jr.; Holm, R. H. *NMR of Paramagnetic Molecules: Principles and Applications*; Academic Press: New York, 1973.

(32) (a) Birnbaum, E. R.; Hodge, J. A.; Grinstaff, M. W.; Schaefer, W. P.; Henling, L.; Labinger, J. A.; Bercaw, J. E.; Gray, H. B. *Inorg. Chem.* **1995**, *34*, 3625–3632. (b) Song, B.; Yu, B.-s. *Bull. Korean Chem. Soc.* **2003**, *24*, 981–985.

(33) Belle, C.; Béguin, C.; Hamman, S.; Pierre, J.-L. *Coord. Chem. Rev.* **2009**, *253*, 963–976.
(34) Motekaitis, R. J.; Martell, A. E. *Inorg. Chem.* **1970**, *9*, 1832–1839.
(35) Thoi, V. S.; Stork, J. R.; Magde, D.; Cohen, S. M. *Inorg. Chem.* **2006**, *45*, 10688–10697.
(36) Hanson, K.; Tamayo, A.; Diev, V. V.; Whited, M. T.; Djurovich, P. I.; Thompson, M. E. *Inorg. Chem.* **2010**, *49*, 6077–6084.
(37) Edwards, P. R.; Johnson, C. E.; Williams, R. J. P. *J. Chem. Phys.* **1967**, *47*, 2074–2082.
(38) The Mössbauer spectrometer operates at liquid nitrogen temperature near 100−120 K.
(39) Drago, R. S. *Physical Methods for Chemists*, 2nd ed.; Harcourt Brace Jovanovich College Publishers: Orlando, FL, 1992.